PCCP

Accepted Manuscript

ROYAL SOCIETY OF CHEMISTRY

www.rsc.org/pccp

Galvanic deposition of Rh and Ru on randomly structured Ti felts for the electrochemical NH_3 synthesis

Kurt Kugler [a], Mareike Luhn [a], Jean André Schramm [a], Khosrow Rahimi [b], Matthias Wessling [a, b, *]

[a] Aachener Verfahrenstechnik – Chemical Process Engineering
RWTH Aachen University
Turmstr. 46, 52064 Aachen, Germany

[b] DWI-Leibniz Institute for Interactive Materials
Forckenbeckstr. 50, 52074 Aachen, Germany

* Prof. Matthias Wessling
Aachener Verfahrenstechnik – Chemical Process Engineering
RWTH Aachen University
Turmstr. 46, 52064 Aachen, Germany
E-mail: manuscripts.cvt@avt.rwth-aachen.de

Abstract

Nowadays NH_3 is exclusively synthesized by the Haber process. Unfortunately, the energy demand and the CO_2 emissions due to H_2 production are high. Hydrogen production utilizes precious carbon sources such as coal and natural gas. In the past we proposed an alternative process concept using a membrane electrode assembly in an electrochemical membrane reactor (ecMR). At the anode H_2O is oxidized at an IrMMO catalyst to form protons. By applying an external potential to the ecMR N_2 is reduced to NH_3 at the cathode. Just recently Rh and Ru were identified as possible cathodic electrocatalysts by DFT calculations. We present an easy and highly efficient method for galvanic coatings of Rh and Ru on randomly structured Ti felts to be used in a membrane electrode assembly. Linear sweep voltammetry measurements give a slightly higher activity of Ru for the liquid phase electrochemical NH_3 synthesis. The reached NH_4^+ concentration is 8 times higher for Ru than for Rh. From an economical point of view, Ru is also more feasible for an electrochemical NH_3 synthesis process. Such electrodes can now be evaluated in an ecMR in comparison to recently demonstrated Ti-based electrodes.

1. Introduction

Ammonia is one of the most important chemicals for the today`s population worldwide. Around 80% of the produced NH_3 are used as fertilizers.[1] Large-scale manufacturing of NH_3 is carried out by the Haber-Bosch process, which suffers from two disadvantages. The process is operated at 150 - 200 bars and 400 - 500°C and around 2 tons CO_2 are emitted per ton produced NH_3 using natural gas for the production of H_2 [2]. Additionally, the Haber-Bosch process is one of the most energy intensive industrial processes contributing 1 - 3% to the global energy demand[3]. Large-scale NH_3 synthesis mainly uses a promoted Fe_3O_4 catalyst. A Ru based catalyst would be more favorable due to its higher catalytic activity. However, the raw material price is too high for a large-scale application and Ru is poisoned by H_2.[4,5]

To overcome the disadvantages of the Haber-Bosch process a more sustainable and potentially cost saving alternative for NH_3 synthesis is desirable. One potential alternative is the application of an electrochemical membrane reactor (ecMR) at ambient conditions [6]. The core of this reactor is a membrane electrode assembly (MEA), which consists of a polymer proton exchange membrane (PEM) and two metal electrodes pressed into the PEM from both sides. Electrical energy, e.g. from renewable energy sources such as wind or solar power, is used as driving force for the chemical reactions taking place at the MEA. Just recently Skúlason et al. identified theoretically possible transition metal catalysts for the electrochemical NH_3 synthesis. Their work gives Fe, Rh and Ru as metals with the highest activity.[7] While Fe is easily accessible in different modifications such as solid plates, powders or felts, Rh and Ru are too expensive to use bulk materials for the manufacturing of electrodes. For an efficient synthesis of NH_3 in the ecMR, a high catalytic surface area at the anode and the cathode is required.

Randomly structured metal felts with certain porosity and high specific surface area are used as electrodes in the ecMR[8]. These metal felts are either directly prepared out of the catalytic material, e.g. Fe, or thin coatings in the range of 1 µm of the desired metals, e.g. Rh and Ru

have to be applied on a proper support material. The support material has to withstand severe conditions, such as corrosion based on the applied direct current or formed anodic O_2, acidic conditions due to the applied H^+ modified PEM and temperatures up to 120 °C[9]. A suitable support material is Ti. In air, a thin around 10 nm thick corrosion resistant TiO_2 layer is formed. Unfortunately TiO_2 has a lower conductivity compared to pure Ti and the surface is quite smooth. For a successful coating the TiO_2 layer has to be removed prior to the coating process by etching with hot concentrated HCl.[10]

In a wide variety of industrial processes such as electronics or the automotive industry electroplating is a key method for preparing thin metal layers. Even though there are many alternatives such as chemical vapor deposition, electroless deposition and atomic layer deposition, electroplating is used nevertheless due to its easy handling and economic aspects. [11] Electroplating on flat Ti surfaces such as discs [12] or foils [13] is a known technique for preparing thin catalyst layers on a corrosion resistant support material. Allen et al. even deposited Pt-based electrocatalysts on regular structured Ti expanded metal meshes by electroplating [14]. However, to the best of our knowledge no research has been reported so far on electroplating on randomly structured Ti felts. This paper aims to give an easy and highly efficient method for galvanic coatings of Rh and Ru on randomly structured Ti felts. Based on polarization curves, the influence of the applied charge, i.e. the applied current and plating time, on the deposition process is investigated. First activity measurements with the coated electrodes are presented and an economical estimation is given, whether Rh or Ru is more feasible for an electrochemical NH_3 synthesis process using an ecMR.

2. Electroplating and parameters

During electroplating of metals solid deposits are formed based on chemical reactions occurring at the surface of conductive materials. The electron charge transfer takes place between the cathode and a metal ion dissolved in an electrolyte.[15] Depending on the use of a soluble or passive anode the concentration of the dissolved metal ions stays constant or decreases in time. For the coating of Rh or Ru a passive anode, e.g. a platinized Ti electrode

is used and the electrolyte has to be replaced or refreshed from time to time for constant plating conditions. Since no oxidation of the anode material occurs, dissolved components of the electrolyte, e.g. SO_4^{2-} ions have to be oxidized.

The main objective of electroplating is to form regular deposits of the desired metal on the support material. Several parameters such as agitation of the electrolyte, temperature, concentration, pH and composition of the electrolyte and the applied current density influence the coating quality and properties.[11] Agitation of the plating bath prevents concentration polarization and gradients in the electrolyte. Depletion of metal ions and formation of pin holes close to the cathode surface are avoided. The morphological structure of deposits is influenced as well. To some extent coarser deposits can be formed and impurities can get embedded.[16,17] Controlling the temperature is crucial for high quality electroplating. In a temperature interval of 5°C around the optimum plating temperature high quality coatings are achieved and sufficient plating rates are accessible. In general a higher temperature leads to a higher plating rate.[17] The composition of the electrolyte affects the appearance of the coating as well. For Cu coatings it is well known that the addition of Cl^- ions leads to a smoother surface with smaller grain size[18] and the coating patterns are spherical[19]. Sulfuric acid is often used as basic solvent for plating baths due to its good conductivity. The coating properties are more affected by the concentration of H_2SO_4 than by the metal ion concentration. Rh coatings can tend to build micro-cracks if the acid concentration is too high[20]. During electroplating sulfate ions undergo a cyclic process. In diluted H_2SO_4 the sulfate ions SO_4^{2-} get oxidized at the anode to SO_4^-. These SO_4^- ions react with H_2O to HSO_4^- and O_2. The HSO_4^- ions dissociate again to SO_4^{2-} and H^+. Finally, these H^+ react at the cathode to form H_2. In total, one H_2O molecule is oxidized, while two SO_4^{2-} ions act as catalyst for the cyclic electrolysis process. Finally, the applied current density has to be matched to the applied temperature and to the electrolyte composition by measuring polarization curves. A low current density will result in a low coating rate and defects in the support material will eventually not be coated at all. Furthermore the deposits contain more impurities and residual stress and changing material properties are the consequences. At

high current densities rough deposits are formed. However, with increasing coating thickness the surface gets smoother. Additionally a high current density does not automatically increase the plating rate, but burned coatings can be formed. At high current densities not only the desired metal ions are reduced, but also H_2 is formed. The formed H_2 can creep underneath a coating layer causing delamination.[11,16] Not only the magnitude of the applied current density is important, but also the current distribution on the electrode surface. Metal ions will not deposit evenly over a large surface, but rather will emerge at preferential domains. The surface of planar support materials develops a certain roughness. There are spots which are closer to the counter electrode, resulting in a localized higher current density. Both, the preferred spots and the localized higher current density, lead to a heterogeneous distribution of the coating on the plating target. A homogeneous electric field parallel to the plating target can support an equal current distribution.[17] Controlling the current density and the current distribution on the electrode surface is crucial for high quality plating results. Considering the nature of randomly structured support materials like the meshes used in this study, obviously the distribution of the coating will be influenced by the heterogeneous distribution of the current.

The mentioned parameters influence the shape and position of the polarization curve measured for a particular electrolyte. A typical polarization curve can be divided in four parts depending on varying rate limiting factors[21,22].

(a) The first part corresponds to the activation or transfer polarization. The applied potential leads to dissociation and ionization of the desired metal. With increasing potential the resulting current density stays close to zero and the process is determined by the kinetics of the electrode reactions. The rate limiting step is the transfer of metal ions through the electrode electrolyte interface.

(b) The second part corresponds to the concentration polarization domain. The applied potential mainly leads to the deposition of metal ions. The number of discharged and deposited ions is rising and the current density and the diffusion rate are increasing as well. The rate limiting step is the depletion of metal ions close to the cathode surface. However,

diffusion limitation increasingly hampers the supply of ions out of the bulk of the solution through the Nernst layer towards the electrode surface.

(c) The third part corresponds to the domain of the limiting current. The current density stays constant at the value of the limiting current density and the ion concentration at the surface has reached a value close to zero. The rate limiting step is the diffusion of metal ions.

(d) The fourth part corresponds to the post limiting region. An additional reaction such as co-deposition or H_2 evolution takes place to further increase the current density. The pH increases at the cathode and metal hydroxides can be incorporated into the metal deposit[17]. The current efficiency decreases and the plating appearance will be rough[22].

By choosing current densities which lie within the second part of the polarization curve, the best plating results should be achieved.

3. Electroplating of Rhodium and Ruthenium

Electroplating of platinum group metals such as Rh and Ru is relevant for high temperature corrosion protection, low resistance contacts and for preparing thin catalyst layers. Rh and Ru catalysts are particular interesting for electrochemical processes such as the electrochemical NH_3 synthesis or the oxidation of H_2O to produce H_2. However, the raw material prices are high and thin electrodeposited catalyst layers are desirable.

3.1 Rhodium

Rhodium is an ideal metal for electrical applications, finishes on scientific and surgical instruments and as contact material in radio frequency circuits since there is no oxide layer present on Rh at ambient conditions.[23] Furthermore deposits of Rh are hard, show low abrasion and are corrosion resistant. According to the volcano plot presented by Skúlason et al.[7] the catalytic activity of Rh and Ru for the electrochemical NH_3 synthesis is comparable. However, Rh is around 17 times more expensive than Ru (see also Table 5)[24].

As early as 1842, H.B. Leeson filed a patent, which announced the possibility of electroplating of Rh[25]. Only 50 years later, July and Leidiè and parallel to them E.F. Smith

tried to electrodeposit Rh for the first time. July and Leidiè found that Rh can not only be deposited from $RhCl_2$ but also from $Rh_2(SO_4)_3$ electrolytes. In 1912 Marino filed a patent for a $RhCl_2$ based electrolyte.[26] However, for technical purposes Rh is usually electrodeposited from sulfate, phosphate or sulfate-phosphate electrolytes today[27].

For Rh coatings, the surface pretreatment is important, since the electrodeposited material shows poor adhesion to the substrate. Cracks in or spalling of the deposit may occur, which is more likely for thick coatings. With rising temperature the tendency for cracking is increasing as well. However, cracks in the deposit can be avoided by electroplating at room temperature[23]. Contrary, the current efficiency increases with temperature, but decreases with decreasing current density.[23,28] Typically Rh is electrodeposited from sulfate electrolytes at the following conditions listed in Table 1.

Table 1: Optimal parameters for the electrochemical deposition of Rh

Parameter	value	reference
pH	< 1	[29]
temperature [°C]	35 -45	[30]
Rh concentration [g/l]	< 4	[26]
current density [A/dm²]	1 - 11	[30]

Electrodeposition of Rh is widely applied on different substrate materials for several applications. Brylev and his co-workers intensively worked on the electrodeposition of Rh on pyrolytic graphite electrodes for the reduction of nitrate and nitrite[31–33]. Several works have been published on the electrodeposition of Rh on Pt electrodes and Pt and Au single-crystals to investigate its electrochemical and electrocatalytic properties, e.g. the adsorption capacity for CO and NO[34–38]. Quite recently, Rh was electrodeposited from ionic liquids by Jayakumar et al.[39,40]. There are also some works on electrodeposition of Rh on Ti substrates[29,41,42], but to the best of our knowledge there are no reports available about electrodeposition of Rh on Ti felts.

3.2 Ruthenium

Being much cheaper than Rh, Ru is even more interesting for the electrochemical NH_3 synthesis. Electrodeposited Ru is hard, has a high wear and arc resistance and shows good electrical conductivity[43–46]. Even at ambient conditions Ru quite readily forms a protective RuO_2 layer. However, in contrast to TiO_2, this oxide layer has the same conductivity as pure Ru[45,47].

Electrodeposition of Ru is a well investigated cheaper method for the preparation of electrical contacts instead of using Au or Rh[46]. In 1936 a patent by Zimmermann and Zschiegner announced the electrochemical deposition of Ru for the first time using various nitrosyl ruthenium complexes[48]. Only 20 years later Volterra was able to electrodeposit Ru on Ag for electrical contacts. However, the formation of toxic RuO_4 at the anode was an undesired parallel reaction[47,49,50]. A detailed investigation of Ru electrolytes was carried out by Reid and Blake[50]. They used a ruthenium nitrosyl sulphamate plating solution which was derived from $RuCl_3$, HNO_3 and $NaHCO_3$ with a valency of Ru of +3. The plating solution was difficult to be prepared reproducible and the reached current efficiencies were less than 20%. With increasing Ru content the current efficiencies got even lower and large scale Ru plating was impossible. In 1969 Reddy and Taimsalu[51] presented a new plating electrolyte based on a well-defined Ru complex, referred to as RuNC. The core is a Ru-N-Ru bridge and the valency of Ru is +4. The reached current efficiencies strongly depend on the operation parameters and electrolyte properties. With increasing pH and temperature the current efficiency increases. Contrary with increasing Ru concentration and current density the current efficiency decreases. The best results were achieved at the following operation parameters (see table 2):

Table 2: Optimal parameters for the electrochemical deposition of Ru[51]

Parameter	value
pH	1.2 - 2.0
temperature [°C]	65 - 85
Ru concentration [g/l]	< 12
current density [A/dm²]	1

Parallel to the work of Reddy and Taimsalu, Bradford, Cleare and Middleton[52] also performed experiments on Ru electroplating using the same Ru complex. Both groups found that the addition of NH_4^+ to the electrolyte or the use of NH_4^+ as counter ions of the Ru complex leads to the suppression of RuO_4 evolution at the anode.

Many studies have been carried out about electroplating of Ru on metal substrates with different goals to be achieved. Electrodeposited Ru or RuO_2 can be used for supercapacitors[53,54], corrosion protection of bipolar plates for polymer electrolyte membrane fuel cells[55] or for the production of electrical contacts [44,45]. Similar to Rh, also the electrochemical deposition of Ru from ionic liquids attracted more attention quite recently[40,56–58]. Due to its corrosion resistance Ti is particularly interesting as support material for Ru coatings. Several works have been published about electroplating of Ru on planar Ti substrates[59–62], but to the best of our knowledge similar to Rh there are no reports available about electrodeposition of Ru on Ti felts.

4. Materials & methods

4.1 Chemicals & Materials

Commercial available Rh and Ru electrolytes (Wieland Edelmetalle GmbH) were used as received for the galvanic coating experiments. The Rh electrolyte consists of $Rh_2(SO_4)_3$ dissolved in H_2SO_4 with a Rh concentration of 2 g/l and a pH < 1. The optimal coating temperature is 20 – 30°C. The Ru electrolyte consists of a Ru complex $(NH_4)_3[\{RuCl_4(H_2O)\}_2(\mu\text{-}N)]$ dissolved in H_2SO_4 with a Ru concentration of 5 g/l and a pH of 1.2 – 1.8. The optimal coating temperature is 60 – 70°C. Randomly structured sintered Ti felts (ST Titanium 15/40, Bekaert Fibre Technologies) with an average fiber diameter of 15 µm, a thickness of 100 µm and a porosity of 40% were used as plating targets. To remove greasy production residues, the Ti felts were pre-cleaned in an ultrasonic bath using an alkaline cleaning bath (Puro S, Wieland Edelmetalle GmbH) according to the manufacturer`s guidelines.

4.2 Pretreatment

The pre-cleaned Ti felts were etched in 20 wt% HCl (ACS reagent, Sigma Aldrich) at 90°C for 4 min. Afterwards the etched Ti felts were electrolytic degreased for 1 min using a cyanide free degreasing solution (WILAPLAT ZFM, Wieland Edelmetalle GmbH) and two stainless steel anodes parallel to the Ti felt. Hydrogen is formed at the surface, in defects and in re-entrant angels and remaining micro contaminations are blasted off. A rough, micro cleaned well wettable surface is achieved. Both the Rh and the Ru electrolytes are strongly acid and corrosion on top of the plating target will occur. Since the surface of the Ti felts was etched prior to each experiment anyway, no protective thin Au or Ni layer from non-corrosive plating baths[46] was electrodeposited prior to the actual coating experiments.

4.3 BET surface measurements

The used Ti felts are randomly structured, thus the specific surface area had to be determined to calculate the resulting current density for the coating experiments. The surface area was measured with a BET device (ASAP 2020, Micromeritics) using Kr as measuring gas. Prior to each measurement the Ti felts were pretreated at 80°C for 60 min under vacuum to desorb adsorbed molecules from the surface. The surface area was calculated using the BET-isotherm. Three samples of each 7 x 7 cm^2 were measured resulting in an average mass related surface area of 717 cm^2/g with a maximum relative deviation of 0.42%. The average specific surface area is 19 m^2/m^2. The Ti felts were not etched prior to the BET measurements. For the calculation of current densities the surface area of the pre-cleaned Ti felts was used.

4.4 Electroplating: Experimental setup and conducted experiments

The coating experiments were conducted in a glass beaker filled with 100 ml electrolyte. The Ru electrolyte was kept at constant temperature of 65°C, while the Rh electrolyte was used at 25°C. Both electrolytes were magnetic stirred at 100 rpm (RCT classic IKAMAG). A potentiostat / galvanostat (PGSTAT302N, Metrohm Autolab) was used as direct current

supply. The square plating target, connected to the working electrode of the potentiostat, had a size of 1.5 x 1.5 cm². At the anode platinized Ti expanded metal electrodes (Wieland Edelmetalle GmbH) were used as insoluble counter electrodes. To achieve homogeneous coating results, two counter electrodes were positioned parallel to the plating target. For polarization measurements an Ag/AgCl reference electrode (Metrohm Autolab) was applied. The duration of each experiment was dependent on the applied current density and the desired charge. To be comparable and for stable operation conditions the plating electrolytes were refreshed regularly.

First both for Rh and Ru polarization curves were measured to identify proper current density regions for successful coatings. For four different chosen current densities varying plating times were calculated based on fixed charge numbers (see Table 3 and 4). Several sets of experiments were conducted to investigate the influence of the applied charge and plating time one the resulting coatings. The plating bath temperature, composition and pH value were not varied.

The mass of the coating layer is proportional to the plating time. At constant current the transferred charge Q increases with increasing plating time. According to Faraday`s law the mass m of a deposited metal can be calculated as:

$$m = \frac{M * Q}{z * F} = \frac{M * I * t}{z * F} \quad (1)$$

where M is the molar mass of the desired metal, F is the Faraday constant equal to 96485 C/mol and z the charge number of the metal ion.[63]

4.5 Analysis of coatings

After etching, the Ti samples were dried at 90°C for 20 min. Following to the coating step the samples were dried again at the same conditions to determine the mass increase. The mass increase was determined using an analytical balance (CPA225D, Sartorius) with an accuracy of 0.01 mg. The morphology and homogeneity of the resulting coatings were analyzed using a scanning electron microscope (S-3000N, Hitachi and DSM 982 Gemini with Field Emission

Gun, Zeiss) with an energy-dispersive spectrometer (Oxford Link ISIS with HPGe detector). To visualize the distribution and to analyze the elemental composition of the coatings on the surface, energy-dispersive X-ray spectroscopy (EDX) measurements were conducted. Furthermore XRD measurements were performed to determine the phase and crystal structure of the deposits. The measurements were done in a PANalytical Empyrean diffractometer at 40 kV and 40 mA. A Cu x-ray tube with a line source of 12 × 0.04 mm^2 provided CuK_α radiation with λ = 0.1542 nm. The K_β line was removed by a Ni filter. Source and detector moved in the vertical direction around a fixed horizontal sample. After passing a divergence slit of 1/8° and an anti-scatter slit of 1/4°, the beam reached the sample at the center of a phi-chi-z stage. In the Bragg-Bretano geometry used, the beam was refocused at a secondary divergence slit of 1/4°. Finally, the signal was recorded by a pixel detector with 256 × 256 pixels of 55 µm as a function of the scattering angle 2θ. Subsequently, the peak positions were calculated from $q = \frac{2\pi}{d} = \frac{4\pi}{\lambda} sin\theta$, in which q is the scattering vector. The detector was used in a scanning geometry that allowed all rows to be used simultaneously. To reduce the background, the divergent beam perpendicular to the scattering plane was controlled by a mask of 4 mm restricting the width of the beam at the sample position to about 10 mm. In addition, the perpendicular divergence was restricted by Soller slits to angles ≤ 2.3°. The scanning was conducted in a range of $2\theta = 30 - 90°$ with a step size of 0.006°. Diffraction patterns were recorded at room temperature. The analysis of the recorded XRD spectra was conducted with the PANalytical software HighScore Software, Version 3.0e.

4.6 Linear sweep voltammetry: Experimental setup and conducted experiments

Linear sweep voltammograms were recorded to determine the activity of the Rh and Ru coatings for the electrochemical NH_3 synthesis. The experiments were conducted in a three-electrode configuration in a closed single-compartment cell at 30°C. The cell was filled with 190 ml of 0.5 M H_2SO_4 (AVS Titrinorm, VWR) as electrolyte. A potentiostat / galvanostat (PGSTAT302N, Metrohm Autolab) was used as direct current supply. The coated felts with a

size of 1.5 x 1.5 cm² were connected to the working electrode. At the anode a platinized Ti expanded metal electrode (Wieland Edelmetalle GmbH) was used as counter electrode and an Ag/AgCl electrode (Metrohm Autolab) was applied as reference electrode. Prior to each experiment the electrolyte was purged with an Ar/H_2 mixture (5 Vol% H_2) to remove dissolved gases. During this purging the working electrode was activated with several cyclic voltammetry runs at a scan rate of 50 mV/s. First three cycles starting at the open circuit potential (OCP) to -0.56 V vs. NHE were measured. Secondly three cycles from -0.56 V vs. NHE to - 1.36 V vs. NHE were performed. Thirdly ten cycles from -1.36 V vs. NHE to the OCP were measured. Finally a chronoamperometry at -0.26 V vs. NHE for 15 min was conducted to polarize the electrode. For the activity measurements for NH_3 synthesis, the electrolyte was purged with a N_2/H_2 mixture (5 Vol% H_2) for 20 min. The linear sweep voltammograms were performed from the OCP to -1.81 V vs. NHE with a sweep rate of 5 mV/s. After the measurement a sample of the electrolyte was taken and the NH_4^+ concentration was determined based on a variation of the Berthelot reaction published by Willis et al.[64].

5. Results

5.1 Pretreatment of randomly structured Ti felts

For successful coatings a rough surface with many re-entrant angles is necessary. Therefore the Ti felts were etched in 20 wt% HCl at 90°C for one to five minutes (see Figure 1) after the pre-cleaning step. With increasing etching time, more TiO_2 gets removed and the surface gets more structured. The grain boundaries and the intergranular material are more affected by the acid than the grain`s surface itself. In the first three minutes mainly intergranular material is removed, whereas in the fourth and fifth minute additionally the grain surface is etched as well. After five minutes the single grains are visible, but the surface roughness has not increased significantly compared to the four minute sample. However, due to the deep intergranular gaps, the mechanical stability of the five minute sample is reduced noticeably.

The etching for four minutes is a compromise between the achieved surface roughness and the mechanical stability of the etched Ti felts.

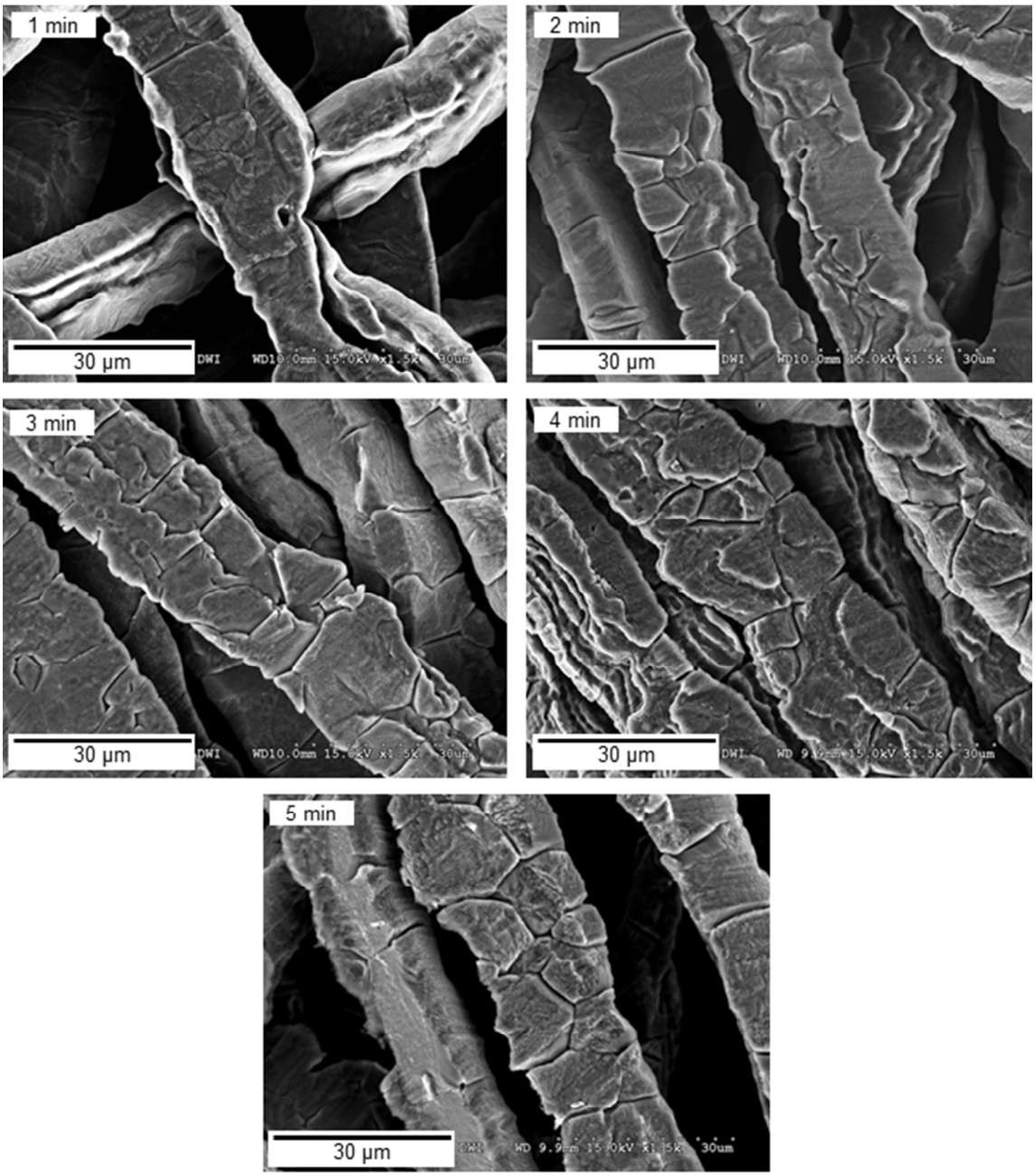

Figure 1: Etched Ti felts in 20 wt% HCl at 90°C for 1 to 5 min.

5.2 Polarization curves for Rh and Ru

Polarization curves for the electroplating of Rh and Ru onto the Ti felts were measured in a three-electrode setup. The working electrode potential was increased by 5 mV for Rh and by

50 mV for Ru every 45 seconds and the resulting current was measured. Figure 2 shows the polarization curves for Rh at 25°C and Ru at 65°C.

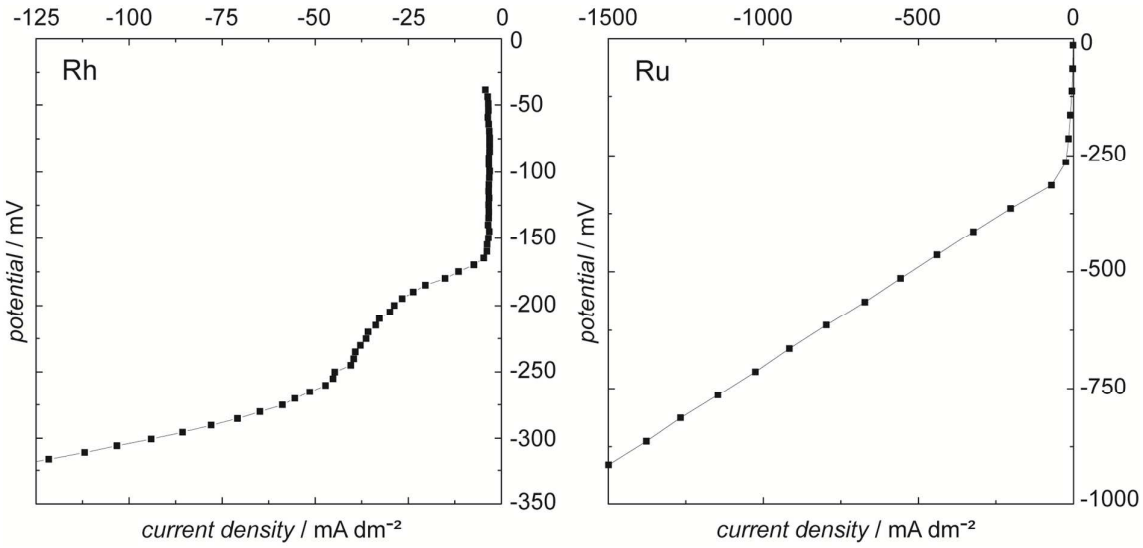

Figure 2: Polarization curves for Rh at 25°C and Ru at 65°C

For Rh the open circuit potential (OCP) is -39 mV and the resulting current density is -4 mA/dm². Beginning at the offset potential of -165 mV the current density is steadily increasing. The resistance of the electrode electrolyte interface was overcome and Rh ions are deposited. At -245 mV the limiting current density of -40 mA/dm² is reached. However, the limiting current region for Rh is little developed only. At -250 mV and a current density of -45 mA/dm² the post limiting region begins and H_2 evolution is a possible undesired parallel reaction. Based on the measured polarization curve, four interesting current densities for the plating experiments were chosen and the corresponding plating times for charges between 3 and 30 C were calculated (see Table 3).

Table 3: Corresponding plating times in seconds for four chosen current densities and fixed charge numbers (each absolute values) for Rh

plating time [s]	current density [mA/dm²]			
charge [C]	12	24	48	96
3	600	300	150	75
6	1200	600	300	150
15	3000	1500	750	375
30	6000	3000	1500	750

The lower two current densities lie in the concentration polarization region of the polarization curve and optimal coating results should be achievable. The third current density is close to the starting point of the post limiting region and the fourth current density lies fully in the H_2 evolution region, meaning the coating quality should be reduced noticeable. In literature optimal current densities of 1 - 4 A/dm² were announced for simple geometries such as plates and wires[23,29,41]. However, the measured polarization curve clearly gives the optimal plating range at current densities below 0.1 A/dm². The lower current densities can be caused by the three dimensional structure of the Ti felts. The felts are quite dense and inner parts may not be coated by Rh at all, resulting in lower currents measured.

Contrary to Rh, for Ru the OCP is +36 mV and the resulting current density is slightly positive being 0.03 mA/dm². At the offset potential of -314 mV the current density increases linearly. A limiting current density was not detectable in the investigated potential range. To make sure that the limiting current region was not overseen, measurements with potential changes of 5 mV and 0.5 mV every 45 seconds respectively were conducted as well. There were no differences in the polarization curves visible. Similar to Rh, also for Ru four current densities were chosen and the resulting plating times were calculated for charge values between 15 and 105 C (see Table 4).

Table 4: Corresponding plating times in seconds for four chosen current densities and fixed charge numbers (each absolute values) for Ru

plating time [s]	current density [mA/dm²]			
charge [C]	115	230	345	460
15	300	150	100	75
45	900	450	300	225
75	1500	750	500	375
105	2100	1050	700	525

All chosen current densities lie within the upper third of the concentration polarization region starting close to the offset current density of around -70 mA/dm². Contrary to Rh, the measured current densities for Ru are in agreement with literature. Park et al. applied current

densities of 300 - 900 mA/dm² to deposit Ru on Ti [59]. Here the felt geometry seems to have no or only little influence on the current densities necessary for plating of Ru.

5.3 Current efficiency, deposited masses, SEM and EDX analysis of Rh

The current necessary to deposit a particular mass m of a desired metal with a current efficiency of 100% can be calculated with the Faraday`s law according to Eq. (1). To calculate the current efficiency of a plating process, this theoretical current is divided by the applied current and multiplied by 100%. The etched Ti samples were dried and weight before and after the plating experiments. The mass difference was used to calculate the theoretically necessary current.

Figure 3 shows the achieved current efficiencies for the plating of Rh as a function of the applied current density for four different charge values between 3 and 30 C.

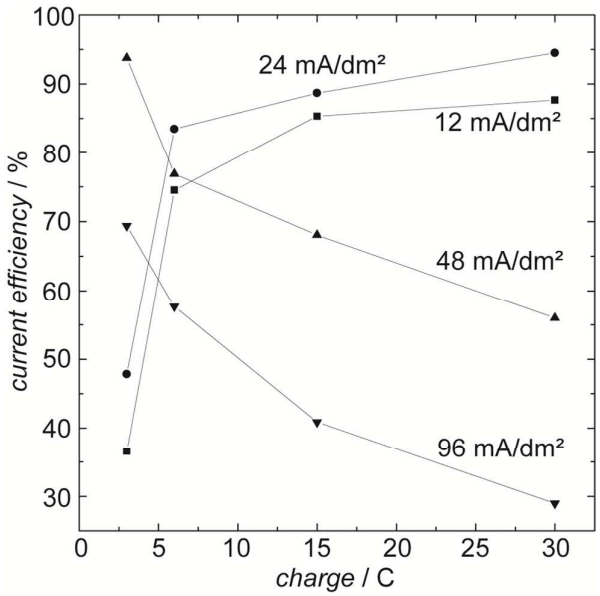

Figure 3: Achieved current efficiencies for the plating of Rh for applied current densities between 12 and 96 mA/dm² and charges between 3 and 30 C (absolute values each)

For the two lower current densities the current efficiency increases logarithmic with increasing charge. The larger the charge, the longer is the plating time and the more Rh molecules are deposited. More precipitation spots are available for following ions to be deposited and the current efficiency is increasing logarithmic. The large difference in current efficiencies for 3 and 6 C shows clearly, that a certain amount of charge is necessary to

achieve a high plating efficiency. At smaller current densities the strength of the electric field between anode and cathode is lower and the diffusion of ions from the bulk to the electrode surface gets limited. Higher charges result in higher current efficiencies. Furthermore for a current density of 24 mA/dm² the current efficiency is also higher than for 12 mA/dm², which is in agreement with literature[23]. At 12 mA/dm² the resistance of the electrode electrolyte interface was not completely overcome, resulting in lower current efficiencies. At 24 mA/dm² the diffusion of the ions is the only limiting factor and with increasing plating time the current efficiency is rising.

Contrary, for the two higher current densities the current efficiency decreases exponentially with increasing charge. Additionally to the deposition of Rh, H_2 evolution is a competing reaction and is lowering the current efficiency and disturbing the deposition process significantly. The longer the plating time, the more predominant the H_2 evolution becomes at the cathode. The more H_2 bubbles are formed, the more cathode surface is blocked and the less Rh can get deposited on the electrode surface. Also at low charge values the negative influence of the H_2 evolution is obvious. The decrease in current efficiency is more regularly than the increase for lower current densities.

The two highest current densities achieved are 94.5% at 24 mA/dm², 30 C and 93.8% at 48 mA/dm², 3C. In literature current efficiencies of around 75% are reported[46]. However, Pletcher et al. also achieved current efficiencies of around 90%[65]. The huge variances in the obtained current efficiencies can be related to the structural features as observed by SEM images (see Figure 4). In the top line of Figure 4 the SEM images for the two highest current efficiencies are shown. Although the two efficiencies are almost equal, the grain structures are completely different. The 48 mA/dm² sample shows a fine micro granular pattern with smaller cracks. However, these cracks reflect only the cracked sub-structure of the Ti substrate after four minutes etching (compare Figure 1). Contrary, the 24 mA/dm² sample shows a highly cracked surface. The single islands of the coating are quite smooth and do not show a granular structure at all. The cracks are deep and go from the surface of the coating down to the Ti substrate. Similar to the 48 mA/dm² sample the 12 and 96 mA/dm²

samples also show a granular structure. Furthermore, the structure of the 96 mA/dm² sample shows a lot of defects and columnar structures. With increasing current density the average grain diameter is increasing as well and the surface gets rougher. According to literature, the surface gets smoother with increasing coating thickness, while at higher current densities a rough surface is formed[16].

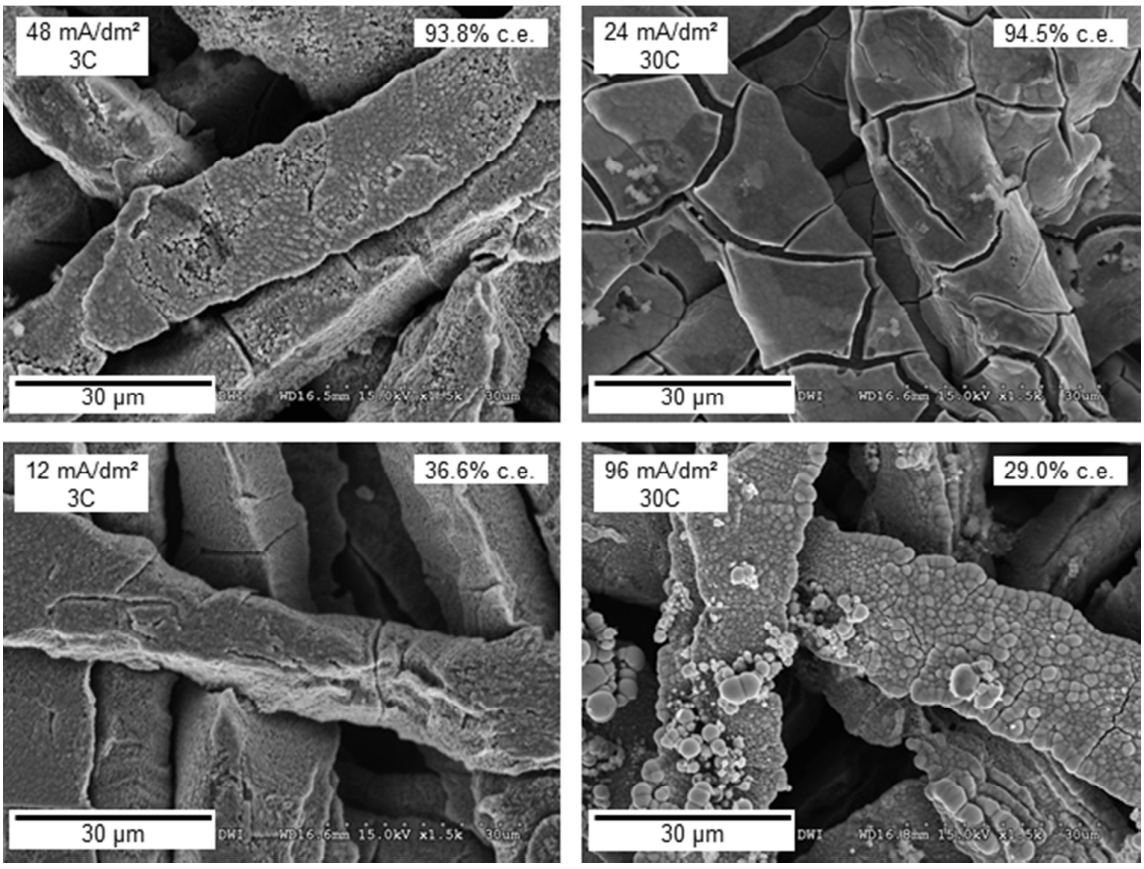

Figure 4: SEM images for Rh coatings at different current densities and charge values. The top line represents the two samples with the highest current efficiencies (c.e.) and the bottom line the two samples with the lowest current efficiencies.

Pushpavanam reports that cracking mainly occurs for thick Rh coatings[23]. When looking at the deposited masses for the different current densities, this suggestion is confirmed (see Figure 5). At 48 mA/dm², 3C 1.0 mg Rh was deposited. Contrary at 24 mA/dm², 30C 10.1 mg Rh were deposited. When assuming that all samples have the same average surface area, the thickness of the coating is increasing with increasing deposited mass. The 24 mA/dm² sample shows the highest mass increase and is also the crack-richest one. As described before, material deposited at lower current densities can obtain impurities which increase

residual stress. Cracks in the coating can be the consequence. Here, the sample coated at the lowest current density shows only minor cracks. However, only 0.4 mg Rh was deposited, resulting in a quite thin coating layer. Thus the structure of the support material is still present.

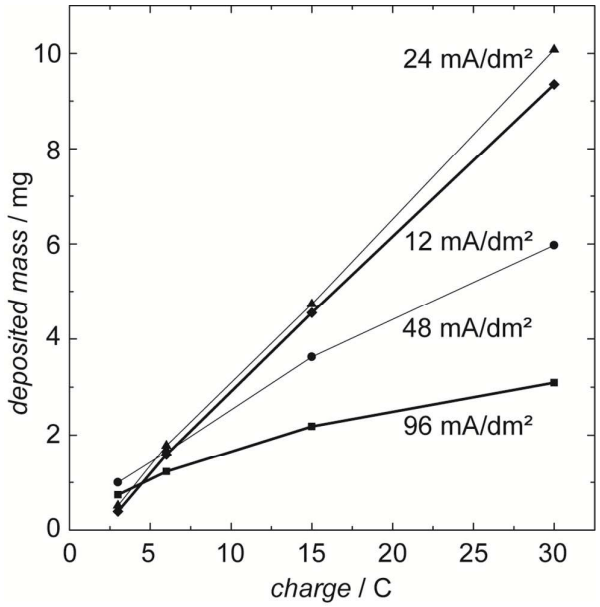

Figure 5: Deposited masses of Rh for different current densities and charge values.

Figure 6 shows the results for EDX measurements for the 48mA/dm², 3C sample with a current efficiency of 93.8%. At the top right of Figure 6 the resulting EDX spectrum is shown. Peaks for C, O, Rh and Ti are visible. The C peak occurs due to the carbon adhesive tape used to fix the samples on the sample holders. Only a small peak for O appears, thus no Rh-O compounds were formed. Since the thickness of the Rh coating is low compared to the diameter of the Ti fibers, a relatively large Ti peak is visible as well. However, the Rh peak is the largest one, which is also confirmed by the EDX mappings shown in the bottom line of Figure 6. On the left the mapping for Rh and on the right the mapping for Ti is shown. Yellow and blue represent the element of interest in each case. The left mapping shows an almost completely closed layer of Rh on top of the support fiber, only minor cracks are visible. On the right the mapping for Ti only shows the corresponding cracks in blue color.

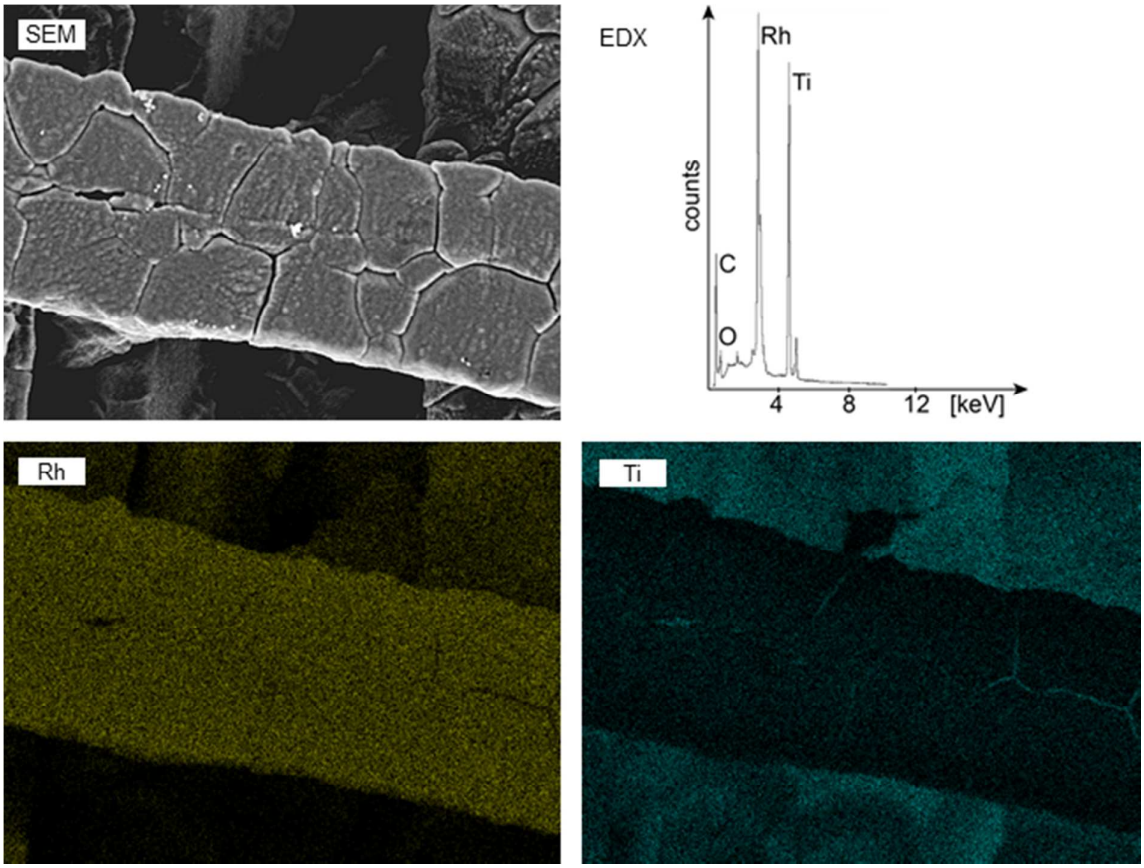

Figure 6: EDX results for a Rh coating at 48 mA/dm² and 3C. Top left shows the SEM image, top right the corresponding EDX spectrum, bottom left EDX mapping for Rh and bottom right EDX mapping for Ti. Yellow and blue represent the element of interest in each case.

5.4 Current efficiency, deposited masses, SEM and EDX analysis of Ru

Figure 7 shows the achieved current efficiencies for the plating of Ru at four different current densities and resulting charge values between 15 and 105 C. For all current densities the current efficiency is rising with rising charge until 75 C.

The longer the plating time, the more Ru molecules can get deposited. However, a further increase in charge beyond 75 C leads to a decrease in current efficiency. At 75 C the current efficiency also decreases with increasing current density. This result is in agreement with the polarization curve for Ru (compare Figure 2). The four chosen current densities all lie within the optimal plating range close to the offset current density. For all current densities the electrical field is strong enough for the deposition of Ru and the resistance of the electrode electrolyte interface was completely overcome. In agreement with literature[51] an increase in

current density only leads to undesired side reactions, which decreases the current efficiency.

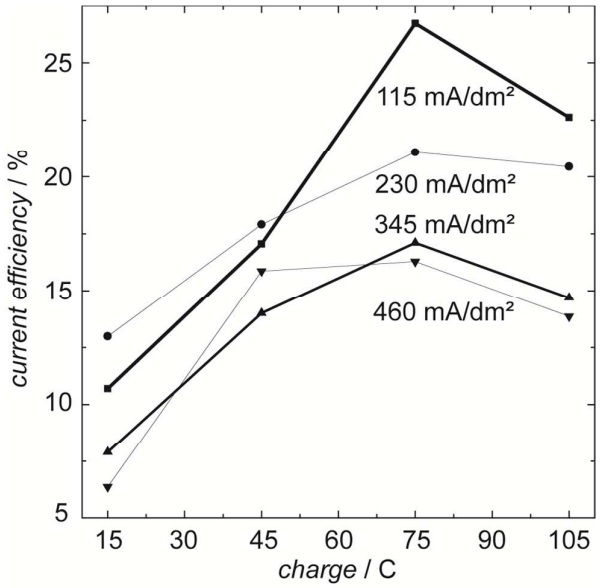

Figure 7: Achieved current efficiencies for the plating of Ru for applied current densities between 115 and 460 mA/dm² and charges between 15 and 120 C (absolute values each)

Contrary to Rh the highest achieved current efficiency for the plating of Ru is only 26.7%. However, Reddy and Taimsalu[51] report current efficiencies of around 90% at a pH of ~ 2. To explain the reduced current efficiency, one has to consider the structure of the Ru complex RuNC being present in the electrolyte. The Ru complex consists of two $RuCl_4$ units bridged by one N atom. For charge neutrality 3 NH_4^+ ions are necessary. Contrary to the Rh electrolyte, which only consists of $Rh_2(SO_4)_3$ dissolved in H_2SO_4, in the Ru electrolyte NH_4^+ ions can react at the cathode as well. Lan and Tao[66] just recently suggested a possible reaction of NH_4^+ at the cathode:

$$2\ NH_4^+ + 2\ O_2 + 2\ e^- \rightarrow N_2 + 4\ H_2O \quad (2)$$

Here O_2 is reduced to H_2O in the presence of NH_4^+, which is oxidized to N_2. This reaction can take place during the electroplating of Ru as well. In each RuNC 2 Ru^{4+} and 3 NH_4^+ ions are present, resulting in a factor of 2/3 for the probability for the reduction of a Ru^{4+} ion. The deviation of four electrons needed for the reduction of Ru^{4+} and only one electron needed for the reaction of one NH_4^+ ion at the cathode is considered when calculating the theoretical deposited mass of Ru with the Faraday law (see Equation 1). The electronegativity (Allred-

Rochow) of O is 3.50, while it is only 1.42 for Ru. This leads to a factor of 142/350 for the affinity of electrons to react with a Ru^{4+} ion. When now multiplying a theoretical efficiency of 100% with these two factors, one get a maximum efficiency of:

100% * 2/3 * 142/350 = 27.05% (3)

Considering this value, the reached efficiency of 26.7% corresponds to a relative efficiency of 98.7%, which is even higher than the current efficiencies reported in literature[51]. To proof the reaction of NH_4^+ at the cathode, the concentration of NH_4^+ ions in the electrolyte before and after a coating step was analyzed using the Berthelot reaction. A strong decrease in NH_4^+ concentration was observed. This observation is in agreement with the notice made by Reddy and Taimsalu[51]. They report that the used Ru electrolyte becomes more acidic during the plating process and that the addition of dilute NH_4OH solution is necessary to keep the pH constant.

Figure 8 shows SEM images for Ru coatings at 75 C for the four chosen current densities between 115 and 460 mA/dm². As expected from the current efficiency curves (see figure 7), the structure of the deposited material gets rougher with increasing current density. The coating gets more irregular and defects get more prevalent. The 115 mA/dm² sample reached the highest current efficiency and also shows the best coating result. The surface is quite smooth and the coating is regular. Compared to the Rh coatings, the structures are finer and the average grain diameter is smaller. According to literature low temperature electrodeposition leads to fine grain structures[46]. Although the Ru electrolyte was operated at 65°C compared to 25°C for the Rh electrolyte, the Ru coating structure is finer than the Rh one. The Rh electrolyte only consists of Rh^{3+} and SO_4^{2-} ions, while the Ru electrolyte also contains Cl^- ions. The phenomenon of smaller coating grains for Ru is similar to the coating of Cu. According to Yao et al.[18] the addition of Cl^- ions leads to a smoother surface with smaller grain size. In agreement with literature the coatings are crack free[51]. The visible gaps in the coating represent the original structure of the Ti substrate after the pretreatment. When looking at the deposited masses for the Ru coating (see Figure 9) this suggestion is confirmed.

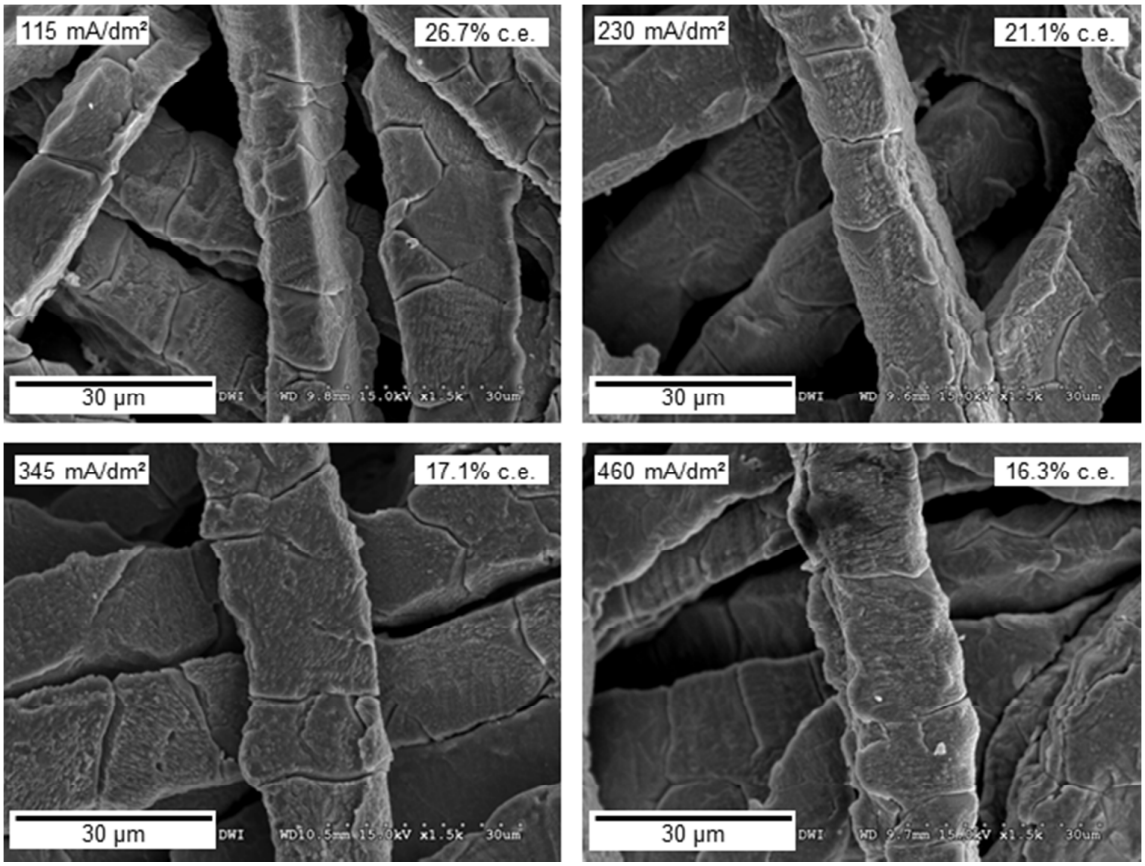

Figure 8: SEM images for Ru coatings at different current densities and a charge of 75 C. For all current densities the highest current efficiency was reached at 75 C.

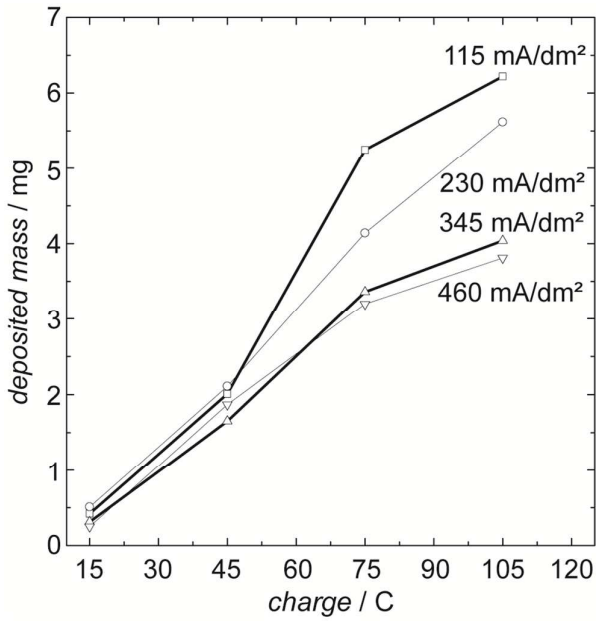

Figure 9: Deposited masses of Ru for different current densities and charge values.

At 115 mA/dm² and 75 C a mass increase of 5.25 mg was observed. Even when assuming that only 10% of the total available area of the Ti substrate was coated, an average coating

thickness of ~1 µm is achieved. With increasing current density the deposited masses get less, thus the average coating thickness is decreasing as well and defects in the coating can be formed. Reddy and Taimsalu give a critical coating thickness of 1.5 µm to obtain crack free coatings[51].

Figure 10 shows the results for EDX measurements for the 115mA/dm², 75 C sample with the highest current efficiency of 26.7%.

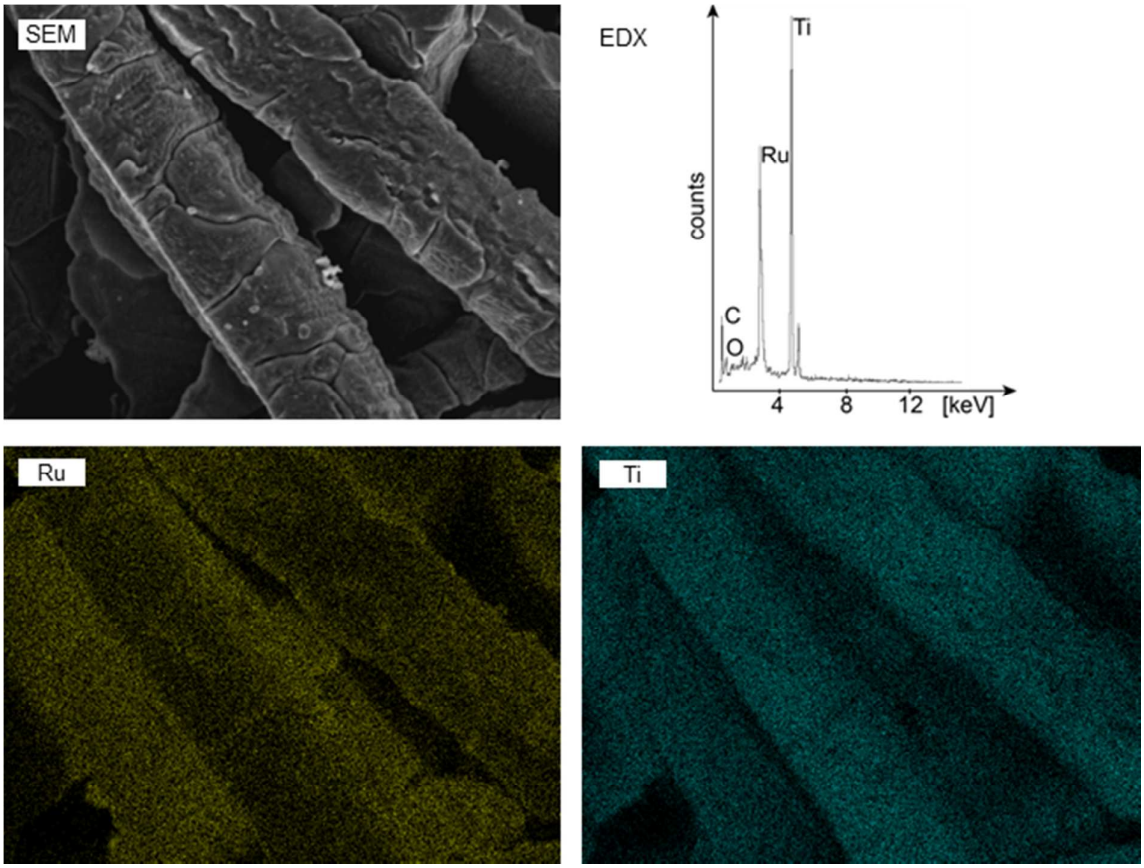

Figure 10: EDX results for a Ru coating at 115 mA/dm² and 75C. Top left shows the SEM image, top right the corresponding EDX spectrum, bottom left EDX mapping for Ru and bottom right EDX mapping for Ti. Yellow and blue represent the element of interest in each case.

At the top right of Figure 10 the resulting EDX spectrum is shown. Similar to the EDX spectrum for Rh peaks for C, O, Ru and Ti are visible. The C peak occurs due to the carbon adhesive tape used to fix the samples on the sample holders. Although Ru quite readily forms RuO_2 at ambient conditions[45,47] only a small peak for O appears, i.e. no Ru-O compounds were formed. Since the thickness of the Ru coating is lower than for the Rh one, the Ti peak is more dominant. This observation is also confirmed by the EDX mappings

shown in the bottom line of Figure 10. On the left the mapping for Ru and on the right the mapping for Ti is shown. Yellow and blue represent the element of interest in each case. The left mapping shows a regular coating of Ru. However, contrary to Rh the coating is quite thin and the background signal of Ti is also visible. The mapping for Ti proofs this statement.

5.5 XRD measurements of coated felts

Figure 11a) and b) show the XRD patterns for an uncoated Ti felt and for felts coated with Rh (a) and Ru (b). The peak identification was carried out by calculating the peak positions with d-spacings for the corresponding primitive cell of the element of interest. The Ti felt was etched for 4 min directly prior to the XRD measurement. The Ti pattern shows primarily peaks for Ti and only few peaks for TiO_2. The patterns for Rh and Ru are quite similar to the Ti pattern.

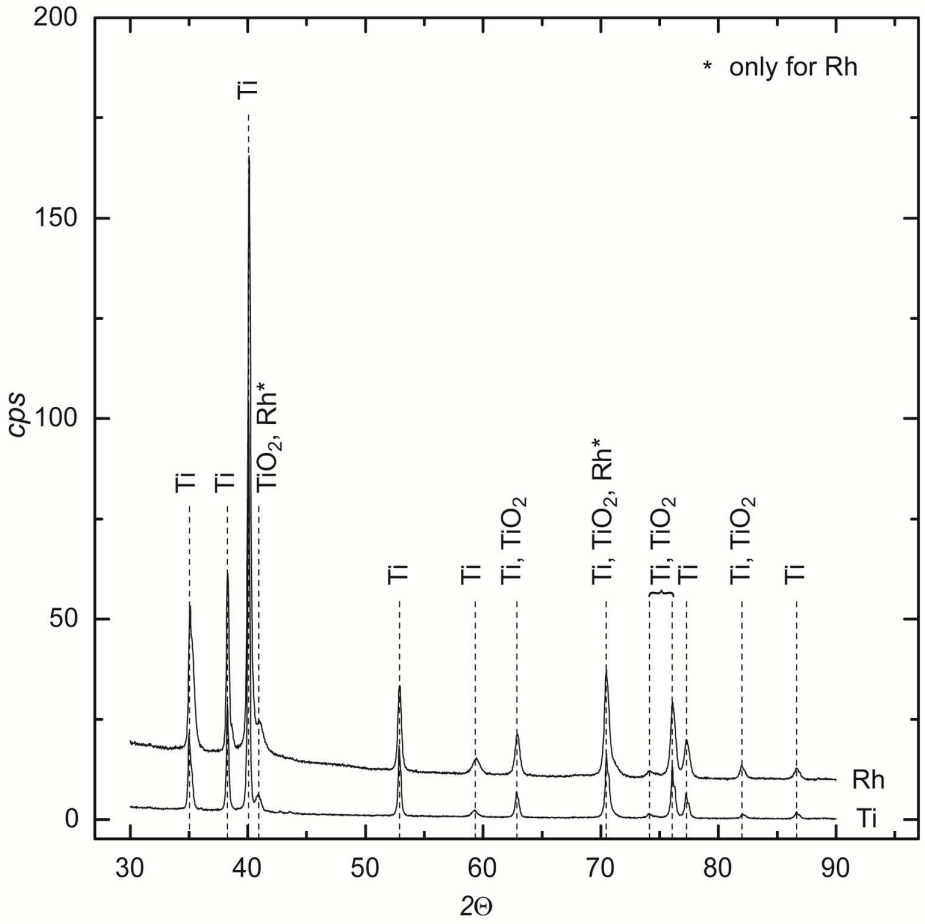

Figure 11a): XRD pattern for a Rh coating on Ti at 48 mA/dm² and 3C. The pattern for Rh is shifted up for visual reason.

The XRD pattern for Rh does not show a specific peak for Rh. However, there are also no peaks apparent for RhO_2, as expected from the EDX results (compare Figure 6). In the Ru pattern there is a single peak for Ru visible at 2Θ = 43.56°. As expected from literature, there are also a few peaks for RuO_2[47]. However the corresponding EDX spectrum (see Figure 10) does not show a dominant O - peak. Most of the Ru, RuO_2 and Rh peaks are overlapping with more dominant Ti peaks. Since the Ru and Rh coatings only have a thickness of around 1 µm, the intensity of the Ti peaks is much stronger. Both the EDX and XRD results prove that Ru and Rh were successfully deposited on the Ti felt.

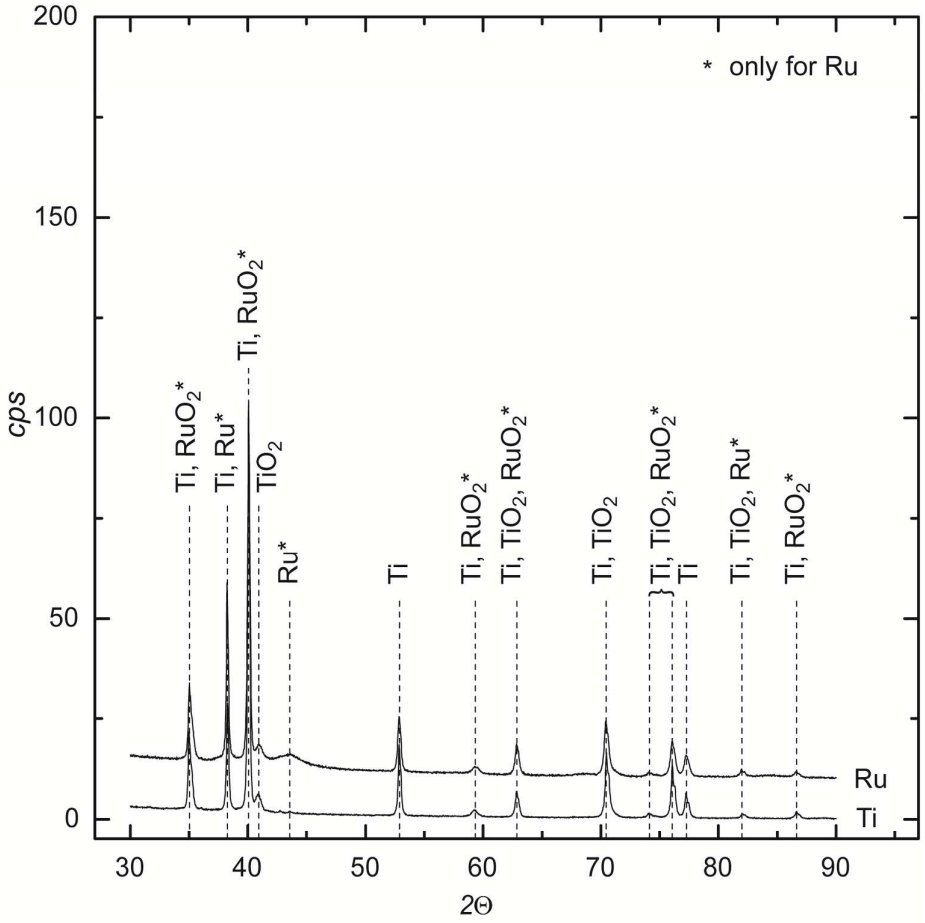

Figure 11b): XRD pattern for a Ru coating on Ti at 115 mA/dm² and 75C. The pattern for Ru is shifted up for visual reason.

5.6 Linear Sweep Voltammetry measurements for Rh and Ru

Linear sweep voltammetry was conducted with Rh and Ru samples coated at the optimal plating conditions (Rh 48 mA/dm² and 3 C, Ru 115 mA/dm² and 75 C). Figure 12a) shows

the linear sweep voltammogram for Rh and Ru electroplated on Ti felts for the electrochemical NH_3 synthesis in liquid phase. For all potentials recorded, the resulting current density is higher for Ru than for Rh. The exact surface area of the coated Rh and Ru felt could not be measured due to lack of material. Therefore the specific surface area of the bare Ti support felt was used to calculate the corresponding current densities for Rh and Ru. The surface area of the Ti felt is assumed to represent the geometric area for the Rh and Ru coatings. In the analyzed potential range no limiting current density was observed.

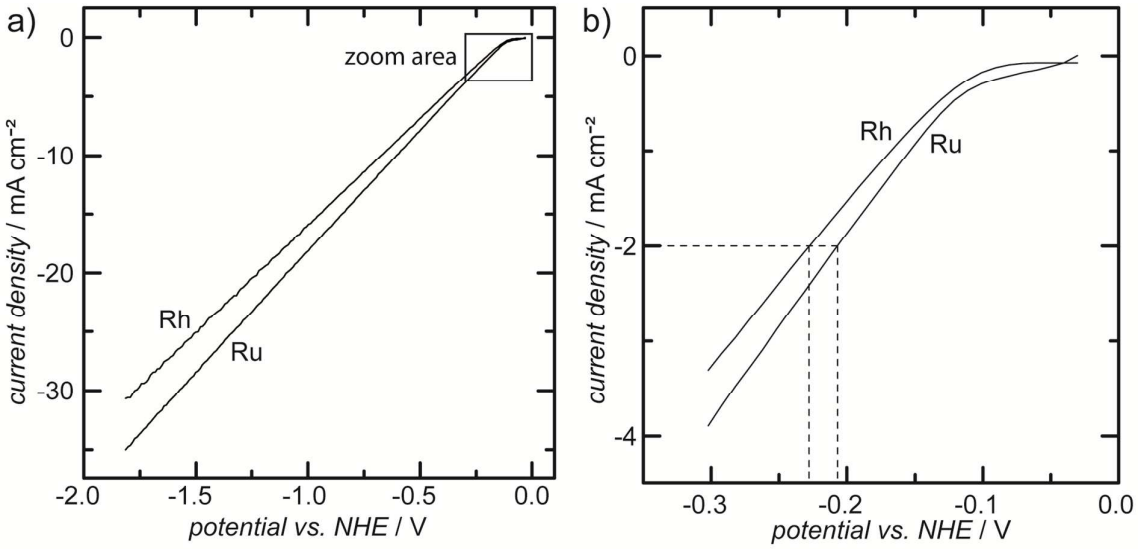

Figure 12: a) Linear sweep voltammogram for Rh and Ru coated Ti felts b) Zoom in to determine the overpotentials of Rh and Ru at a current density of 2 mA/cm² for the electrochemical NH_3 synthesis

A parameter for the activity of a catalyst for a desired reaction is the overpotential η at a particular current density. Miles et al. defined a current density of 2 mA/cm² as reasonable[67]. The lower the overpotential is, the higher is the activity of the catalyst for the investigated reaction. Figure 12b) shows a zoom in for the potential range of 0.0 to -0.3 V vs. NHE to determine the overpotentials for Rh and Ru for the electrochemical NH_3 synthesis. The overpotential is defined as the difference between the measured potential and the standard potential of the desired reaction. The standard potential of the electrochemical NH_3 synthesis is $E^0_{NH3} = -0.057V\ vs.\ NHE$[68]. For the applied reaction conditions Rh has a slightly higher overpotential than Ru. The values are η_{Rh} = 171 mV and η_{Ru} = 150 mV. The activity of the Ru coating should be higher than the one of the Rh coating. This assumption is confirmed by analysis of the samples taken after the measurement. The NH_4^+ concentration in the

electrolyte was 0.07 mg/l for Rh and 0.58 mg/l for Ru corresponding to production rates of $1.5*10^{-11}$ mol s^{-1} cm^{-2} for Rh and $1.2*10^{-10}$ mol s^{-1} cm^{-2} for Ru. The values for the standard deviation for the NH_4^+ concentration are 3.9% for Rh and 0.3% for Ru. Contrary to the predictions of Skúlason et al.[7], the activity of Rh should be slightly higher than the one of Ru. There are a few works reported in literature on the electrochemical synthesis of NH_3 in liquid phase by Furuya and Hoshiba[69–71], Tsuneto et al.[72,73] and Köleli and Röpke[74,75]. Production rates between $6.3*10^{-12}$ [75] and $6.4*10^{-9}$ mol s^{-1} cm^{-2} [71] were achieved. However, complex metal phthalocyanine cathodes[69–71], organic solvents mediated by $LiClO_4$[72,73] or Pt electrodes coated with polyaniline or polypyrrole at high N_2 pressures of up to 50 bars[74,75] were used. Apparently, we find comparable production rates but our electrochemical cell used here comprises an ordinary three electrode configuration and an aqueous electrolyte.

5.7 Economical estimation

To answer the question whether Rh or Ru as potential cathodic catalyst in an ecMR is more feasible, several aspects have to be considered. The first aspect relates to the costs for an efficient plating of Rh and Ru. Table 5 gives an overview about cost relevant numbers.

Table 5: Price comparison of Ru and Rh coatings

Parameter	Ru	Rh
mass [mg]	5.25	1.0
price [€/g] [24]	2.15	35.5
plating time [s]	1500	150
consumed power [10^{-6} kWh]	6.9	0.2
factor materials costs Ru/Rh	31.8	

At the two highest current efficiencies of 93.8% for Rh and 26.7% for Ru, 5.25 mg of Ru and 1.0 mg of Rh were deposited. However, as mentioned before, Rh is much more expensive than Ru. The plating time for Ru is ten times longer than for Rh. When considering the necessary current and the resulting potential values, plating of Ru consumes ~35 times more power than plating of Rh. However, the costs for electricity are significantly lower than the raw material costs for Rh and Ru. The material costs for a Ru coating at the given

parameters are only around one third of the costs for a Rh coating. Since the material densities for Rh and Ru are almost equal being 12.38 and 12.37 g/cm^3 [46], the costs for a deposited layer with a particular thickness are much cheaper for Ru. Considering the higher activity of Ru and the higher concentration of NH_4^+ reached during the linear sweep voltammetry measurements, Ru is superior to Rh for the electrochemical NH_3 synthesis. This analysis is based on the assumption that liquid phase catalysis proceeds following the same principles as a gas phase catalysis using our proposed membrane electrode assembly in an electrochemical membrane reactor. This needs to be analyzed and verified through systematic electrochemical characterization.

6. Conclusion

In this work we presented an easy and highly efficient method for galvanic coatings of Rh and Ru on randomly structured Ti felts. Due to the random structure of the Ti felts, the pretreatment with 20 wt% HCl was optimized. Based on polarization curves, proper plating were identified. The current necessary for a successful and high quality coating of Ru is much higher than for Rh. The optimal current density for Ru was 115 mA/dm², while for Rh 48 mA/dm² was applied. The investigated current density values are in agreement with literature for Ru. However, for Rh much higher values of 1 - 4 A/dm² are reported. The successful coatings were proved both for Rh and Ru by SEM/EDX and XRD measurements. Both for Rh and for Ru high current efficiencies of 93.8% and 98.7% respectively were achieved. The activity of the Rh and Ru coatings for the electrochemical NH_3 synthesis was confirmed by linear sweep voltammetry measurements. The voltammograms give a slightly higher activity for Ru, which was confirmed by a higher NH_4^+ concentration in the electrolyte after the measurement. From an economic point of view Ru is also more interesting for an electrochemical NH_3 synthesis process, since the total costs for a Ru coating are only around 1/3 of the costs related to Rh. For a future electrochemical NH_3 synthesis processes Ru can play an important role as catalyst material, since the presented plating method is highly efficient and cost-saving.

7. Acknowledgement

This work was performed in part at the Center for Chemical Polymer Technology CPT, which is supported by the EU and the federal state of North Rhine-Westphalia (grant no. EFRE 30 00 883 02).

References

1. V. Smil, *Nature*, 1999, **400**, 415.

2. I. Rafiqul, C. Weber, B. Lehmann, and A. Voss, *Energy*, 2005, **30**, 2487–2504.

3. M. Appl, in *Ullmann's Encyclopedia of Industrial Chemistry*, Wiley-VCH Verlag GmbH & Co. KGaA, Weinheim, 2006.

4. Huazhang Liu, *Ammonia Synthesis Catalysts - Innovation and Practice*, World Scientific Publishing Co. Pte. Ltd., 2013.

5. M. Kitano, Y. Inoue, Y. Yamazaki, F. Hayashi, S. Kanbara, S. Matsuishi, T. Yokoyama, S.-W. Kim, M. Hara, and H. Hosono, *Nat. Chem.*, 2012, **4**, 934–940.

6. K. Kugler, B. Ohs, M. Scholz, and M. Wessling, *Phys. Chem. Chem. Phys.*, 2014, **16**, 6129–6138.

7. E. Skúlason, T. Bligaard, S. Gudmundsdóttir, F. Studt, J. Rossmeisl, F. Abild-Pedersen, T. Vegge, H. Jónsson, and J. K. Nørskov, *Phys. Chem. Chem. Phys.*, 2012, **14**, 1235–1245.

8. S. M. A. Kriescher, K. Kugler, Y. Gendel, S. S. Hosseiny, and M. Wessling, *Electrochem. commun.*, in press.

9. E. M. Gabreab, G. Hinds, S. Fearn, D. Hodgson, J. Millichamp, P. R. Shearing, and D. J. L. Brett, *J. Power Sources*, 2014, **245**, 1014–1026.

10. J. Matthew J. Donachie, *Titanium - A Technical Guide*, ASM International, 2000.

11. M. Schlesinger and M. Paunovic, Eds., *Modern Electroplating*, John Wiley & Sons, Inc., Hoboken, New Jersey, USA, 2010.

12. T. M. Manhabosco and I. L. Muller, *Appl. Surf. Sci.*, 2009, **255**, 4082–4086.

13. G. F. Ortiz, M. C. López, R. Alcántara, and J. L. Tirado, *J. Alloys Compd.*, 2014, **585**, 331–336.

14. R. G. Allen, C. Lim, L. X. Yang, K. Scott, and S. Roy, *J. Power Sources*, 2005, **143**, 142–149.

15. A. A. Pasa and M. L. Munford, in *Encyclopedia of chemical processing*, Taylor & Francis Group, New York, USA, 2006.

16. T. Bergstresser and H. Merchant, in *Defect structure, Morphology and Properties of Deposits*, ed. H. Merchant, The Minerals, Metals & Materials Society, 1995.

17. M. Paunovic and M. Schlesinger, Eds., in *Fundamentals of electrochemical deposition*, John Wiley & Sons, Inc., Hoboken, New Jersey, USA, 2006.

18. Y. Yao, *Trans. Electrochem. Soc.*, 1944, **86**, 371–382.

19. S. C. Barnes, *Electrochim. Acta*, 1961, **5**, 79–86.

20. F. H. Reid, in *Gmelin handbook of inorganic chemistry: System Number 68. Pt, Platinum. Technology of platinum-group metals*, Springer, 1986, pp. 66–91.

21. M. Paunovic and M. Schlesinger, in *Fundamentals of Electrochemical Deposition*, eds. M. Paunovic and M. Schlesinger, John Wiley & Sons, Inc., Hoboken, New Jersey, USA, 2006.

22. J. B. Mohler, *Electroplating and Related Processes*, Chemical Publishing Co., Inc. New York, 1969.

23. M. Pushpavanam, V. Raman, and B. A. Shenoi, *Surf. Technol.*, 1981, **12**, 351–360.

24. www.agosi.de, *accessed 05th Sept. 2014*, 2014.

25. P. D. Buchanan, *Platin. Met. Rev.*, 1981, **25**, 32–41.

26. E. R. Thews, *Metalloberfläche*, 1956, **10**, 85–89.

27. F. H. Reid, *Metall. Rev.*, 1963, **8**, 167–211.

28. L. Serota, *Met. Finish.*, 1966, **64**, 82–84.

29. A. M. Baraka, H. H. Shaarawy, and H. A. Hamed, *Anti-Corrosion Methods Mater.*, 2002, **49**, 277–282.

30. K. Schumpelt, *Trans. Electrochem. Soc.*, 1941, **80**, 489–498.

31. O. Brylev, L. Roué, and D. Bélanger, *J. Electroanal. Chem.*, 2005, **581**, 22–30.

32. O. Brylev, M. Sarrazin, D. Bélanger, and L. Roué, *Appl. Catal. B Environ.*, 2006, **64**, 243–253.

33. O. Brylev, M. Sarrazin, L. Roué, and D. Bélanger, *Electrochim. Acta*, 2007, **52**, 6237–6247.

34. R. T. S. Oliveira, M. C. Santos, L. O. S. Bulhões, and E. C. Pereira, *J. Electroanal. Chem.*, 2004, **569**, 233–240.

35. J. Inukai and M. Ito, *J. Electroanal. Chem.*, 1993, **358**, 307–315.

36. F. J. Gutiérrez de Dios, R. Gómez, and J. M. Feliu, *Electrochem. commun.*, 2001, **3**, 659–664.

37. R. Gómez and J. M. Feliu, *Electrochim. Acta*, 1998, **44**, 1191–1205.

38. M. Arbib, B. Zhang, V. Lazarov, D. Stoychev, and A. Milchev, 2001, **510**, 67–77.

39. M. Jayakumar, K. A. Venkatesan, and T. G. Srinivasan, *Electrochim. Acta*, 2008, **53**, 2794–2801.

40. M. Jayakumar, K. A. Venkatesan, R. Sudha, T. G. Srinivasan, and P. R. Vasudeva Rao, *Mater. Chem. Phys.*, 2011, **128**, 141–150.

41. M. Vukovic, *J. Electroanal. Chem.*, 1988, **242**, 97–105.

42. M. Vukovic and D. Cukman, *J. Electroanal. Chem.*, 1992, **333**, 195–203.

43. T. Jones, *Met. Finish.*, 2001, **99**, 121–128.

44. Anon., *Plat. Surf. Finish.*, 1984, **73**, 26–28.

45. T. A. Palumbo, *Plat. Surf. Finish.*, 1979, **66**, 42–44.

46. C. Rao and D. Trivedi, *Coord. Chem. Rev.*, 2005, **249**, 613–631.

47. B. P. C. Hydes, 1980, 50–55.

48. F. Zimmermann and H. Emil, 1936, 55–58.

49. R. U. Volterra, 1952, 2–3.

50. F. H. Reid and J. C. Blake, *Trans. Inst. Met. Finish.*, 1961, **38**, 45–51.

51. G. S. Reddy and P. Taimsalu, *Trans. Inst. Met. Finish.*, 1969, **47**, 187–193.

52. B. C. W. Bradford, M. J. Cleare, and D. I, 1969, 90–92.

53. V. D. Patake, C. D. Lokhande, and O. S. Joo, *Appl. Surf. Sci.*, 2009, **255**, 4192–4196.

54. J. M. Sieben, E. Morallón, and D. Cazorla-Amorós, *Energy*, 2013, **58**, 519–526.

55. K. M. Kim, J. H. Kim, Y. Y. Lee, and K. Y. Kim, *Int. J. Hydrogen Energy*, 2012, **37**, 1653–1660.

56. O. Mann, W. Freyland, O. Raz, and Y. Ein-Eli, *Chem. Phys. Lett.*, 2008, **460**, 178–181.

57. O. Raz, G. Cohn, W. Freyland, O. Mann, and Y. Ein-Eli, *Electrochim. Acta*, 2009, **54**, 6042–6045.

58. M. Jayakumar, K. A. Venkatesan, T. G. Srinivasan, and P. R. Vasudeva Rao, *Electrochim. Acta*, 2009, **54**, 6747–6755.

59. B.-O. Park, C. D. Lokhande, H.-S. Park, K.-D. Jung, and O.-S. Joo, *Mater. Chem. Phys.*, 2004, **87**, 59–66.

60. Y.-Z. Zheng, H.-Y. Ding, and M.-L. Zhang, *Thin Solid Films*, 2008, **516**, 7381–7385.

61. J.-J. Jow, H.-J. Lee, H.-R. Chen, M.-S. Wu, and T.-Y. Wei, *Electrochim. Acta*, 2007, **52**, 2625–2633.

62. Y.-S. Kim, H.-I. Kim, J.-H. Cho, H.-K. Seo, G.-S. Kim, S. G. Ansari, G. Khang, J. J. Senkevich, and H.-S. Shin, *Electrochim. Acta*, 2006, **51**, 5445–5451.

63. A. J. Bard and L. R. Faulkner, *Electrochemical Methods - Fundamentals and Applications*, John Wiley & Sons, Inc., U.K., 2010.

64. R. B. Willis, M. E. Montgomery, and P. R. Allen, 1996, **0003**, 1804–1807.

65. D. Pletcher and R. I. Urbina, *J. Electroanal. Chem.*, 1997, **421**, 145–151.

66. R. Lan and S. Tao, *ECS Electrochem. Lett.*, 2013, **2**, F37–F40.

67. M. H. Miles, E. A. Klaus, and B. P. Gunn, 1977.

68. M. Pourbaix, *Atlas of Electrochemical Equilibria in Aqueous Solutions*, NACE International Cebelcor, Second Eng., 1974.

69. N. Furuya and H. Yoshiba, *J. Electroanal. Chem. Interfacial Electrochem.*, 1989, **263**, 171–174.

70. N. Furuya and H. Yoshiba, *J. Electroanal. Chem. Interfacial Electrochem.*, 1989, **272**, 263–266.

71. N. Furuya and H. Yoshiba, *J. Electroanal. Chem. Interfacial Electrochem.*, 1990, **291**, 269–272.

72. A. Tsuneto, A. Kudo, and T. Sakata, *Chem. Lett.*, 1993, 851–854.

73. A. Tsuneto, A. Kudo, and T. Sakata, *J. Electroanal. Chem.*, 1994, **367**, 183–188.

74. F. Köleli and T. Röpke, *Appl. Catal. B Environ.*, 2006, **62**, 306–310.

75. F. Köleli and D. B. Kayan, *J. Electroanal. Chem.*, 2010, **638**, 119–122.